coatings

Article

The Impurity and Decay-Magnetic Polaron Effects in III–V Compound Gaussian Quantum Wells

Xin Zhang, Wei Zhang, Xin-Jun Ma, Pei-Fang Li, Yong Sun * and Jing-Lin Xiao *

Institute of Condensed Matter Physics and College of Mathematics and Physics, Inner Mongolia Minzu University, Tongliao 028043, China; zhangxin1006@126.com (X.Z.); 15771555013@163.com (W.Z.); maxiaoguang80@126.com (X.-J.M.); lipeifang82@163.com (P.-F.L.)
* Correspondence: sy19851009@126.com or sunyong@imun.edu.cn (Y.S.); xiaojlin@126.com (J.-L.X.)

Abstract: The effects of a decay magnetic field and hydrogen-like impurities on the ground-state binding energy (GSBE) and ground-state energy (GSE) of weak-coupling bound polarons in asymmetrical Gaussian potential (AGP) III–V compound quantum wells (QWs) were studied based on unitary transformation methods and linear combination operators. By numerical calculation, we found that the polarons were affected by the AGP, the decay magnetic field, Coulomb impurities, and the type of crystal, which led to a series of interesting phenomena, such as changes in the ground-state energy and the ground-state binding energy. The results obtained provide good theoretical guidance for optoelectronic devices and quantum information.

Keywords: asymmetric Gaussian confinement; III–V compound semiconductor; polaron; hydrogen-like impurity; decay magnetic field; quantum well

Citation: Zhang, X.; Zhang, W.; Ma, X.-J.; Li, P.-F.; Sun, Y.; Xiao, J.-L. The Impurity and Decay-Magnetic Polaron Effects in III–V Compound Gaussian Quantum Wells. *Coatings* **2022**, *12*, 1072. https://doi.org/10.3390/coatings12081072

Academic Editor: Aomar Hadjadj

Received: 26 June 2022
Accepted: 27 July 2022
Published: 29 July 2022

1. Introduction

In low-dimensional semiconductors, especially in quantum dots [1,2], quantum rods [3], quantum wires [4,5], and quantum wells (QWs) [6,7], there are obvious electron–phonon interactions, which produce quasi-particles called polarons. In recent years, since polarons have critical influence on the photoelectric characteristics of materials, research on polarons has become increasingly popular among researchers. Therefore, many researchers have conducted theoretical and experimental studies on the polaron effect in QWs [8]. In theoretical studies, researchers have presented a variety of methods, including effective mass approximation [9], perturbation theory [10], the variational method [11], the iterative method [12], and the compact-density-matrix approach [13], to investigate polarons in QWs. In experimental studies, researchers have applied several methods to investigate polarons in QWs. For example, Frankerl et al. [14] performed low-temperature time-resolved photoluminescence (PL) experiments and found that strong carrier decay time variations with detection photon energy prove a significant effect of carrier localization, depending primarily on the width of the QW. Gusev et al. [15] observed both topological insulator and gapless semimetal phases, based on theoretical predictions and depending on sample parameters, through investigating nonlocal and local resistance in HgTe-based double QWs. Donmez et al. [16] performed magnetotransport measurements to evaluate the influences of thermal annealing and Bi on the electronic transport characteristics of n-type modulation-doped AlGaAs/GaAsBi QWs. These research works evaluated the effects of different parameters, such as the magnetic field [17], electric field [18], hydrogen-like impurity field [19], temperature [20], and laser field [21], and found that only one or two of them had important influences on polarons in QWs.

Polaron properties are greatly affected by both a non-uniform magnetic field and hydrogen-like impurities. In fact, this is a common situation in the experiments and processing of QW devices. Therefore, studying polaron non-uniform magnetic fields and hydrogen-like impurity effects on the photoelectric properties of QWs is of great importance.

However, no research has been conducted on hydrogen-like impurity effects on weak-coupling bound-magneto-polaron properties in AGCPQWs using unitary transformation and linear combination operator methods.

We investigated the AGP range and hydrogen-like impurity effects on the ground-state energy (GSE) and ground-state binding energy (GSBE) of weak-coupling bound-magneto-polarons in AGP III–V compound QWs (see Figure 1). It was found that the self-parameters of QWs, coupling-parameters, hydrogen-like impurities, and decay magnetic field are vital for polaron effects in nanostructures.

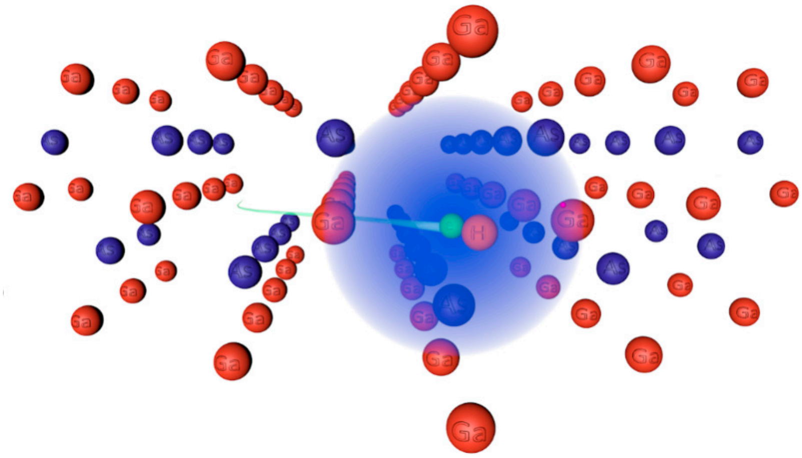

Figure 1. Schematic diagram of a polaron with a hydrogenic impurity in an asymmetric Gaussian potential QW.

2. Theoretical Method

In this section, we considered an electron confined in an AGCPQW that moves in a GaAs semiconductor crystal and interacts with bulk longitudinal optical (LO) phonons in a decay magnetic field. According to effective mass approximations, the electron–phonon system Hamiltonian in the presence of hydrogen-like impurities at the coordinate origin could be expressed as [19]

$$
\begin{aligned}
H = {} & \frac{1}{2m}\left(p_x - \frac{\overline{\beta}^2}{4}y\right)^2 + \frac{1}{2m}\left(p_y + \frac{\overline{\beta}^2}{4}x\right)^2 + \frac{p_z^2}{2m} + \sum_{\mathbf{q}} \hbar\omega_{LO} a_{\mathbf{q}}^{\dagger} a_{\mathbf{q}} \\
& + \sum_{\mathbf{q}} \left[V_q a_{\mathbf{q}} \exp(i\mathbf{q}\cdot\mathbf{r}) + h.c\right] + V(z) - \frac{\eta}{r},
\end{aligned}
\tag{1}
$$

$$
V(z) = \begin{cases} -V_0 \exp\left(-\dfrac{z^2}{2R^2}\right) & z \geq 0 \\ \infty & z < 0 \end{cases}
\tag{2}
$$

$$
\overline{\beta}^2 = 2eB/c
\tag{3}
$$

$$
\begin{aligned}
V_q &= i\left(\frac{\hbar\omega_{LO}}{q}\right)\left(\frac{\hbar}{2m\omega_{LO}}\right)^{\frac{1}{4}}\left(\frac{4\pi\alpha}{V}\right)^{\frac{1}{2}}, \\
\alpha &= \left(\frac{e^2}{2\hbar\omega_{LO}}\right)\left(\frac{2m\omega_{LO}}{\hbar}\right)^{\frac{1}{2}}\left(\frac{1}{\varepsilon_\infty} - \frac{1}{\varepsilon_0}\right),
\end{aligned}
\tag{4}
$$

where β is the parameter related to the magnetic field, m is the band mass of the electron, and $a_{\mathbf{q}}^{\dagger}$ $(a_{\mathbf{q}})$ is the creation (annihilation) operator of LO phonons with frequency ω_{LO}. $\mathbf{p}$ and $\mathbf{r}$ are momentum and position vectors for electrons, respectively. $V(z)$ is the AGCP along the z direction representing the AGCPQW growth direction [22–24], V_0 is the AGCPQW barrier height, R is the AGCP range, and η is the Coulombic impurity potential strength that satisfies $\eta = e^2/\varepsilon_0$. In addition, the decay magnetic field shown in Figure 2 can be expressed as

$$B = \frac{B_0 \exp(-\omega t)}{C}, \tag{5}$$

where B_0 is the initial magnetic induction intensity; ω and t are the decay frequency and the decay time of the magnetic field, respectively; and C is a dimensionless parameter whose default value is chosen as $C = 0.05$.

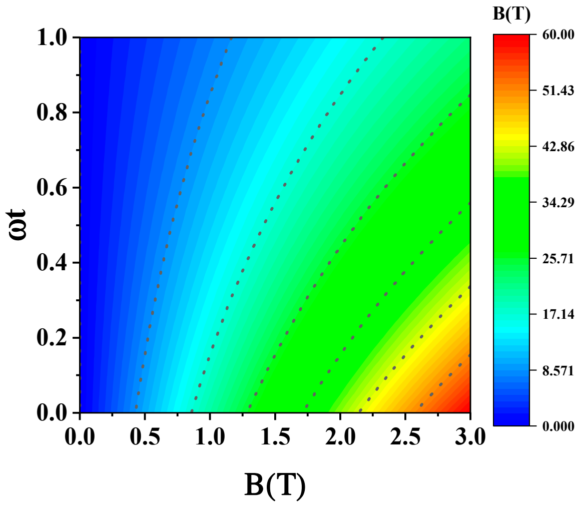

Figure 2. Schematic diagram of a decay magnetic field.

Employing Fourier expansion to the Coulomb-bound potential, it can be written as

$$-\frac{e^2}{\varepsilon_0 r} = -\frac{4\pi e^2}{\varepsilon_0 \nu} \sum_{\mathbf{q}} \frac{1}{q^2} \exp(-i\mathbf{q}\cdot\mathbf{r}) \tag{6}$$

To compute the Hamiltonian, it needs to be quantized. Therefore, Equation (1) was carried out by two unitary transformations [25,26]:

$$U_1 = \exp\left(-i\sum_{\mathbf{q}} \hbar\mathbf{q} \cdot \mathbf{r} a_{\mathbf{q}}^{\dagger} a_{\mathbf{q}}\right), \tag{7}$$

$$U_2 = \exp\left(\sum_{\mathbf{q}} \left(a_{\mathbf{q}}^{\dagger} f_q - a_{\mathbf{q}} f_q^*\right)\right), \tag{8}$$

where $f_q\left(f_q^*\right)$ is a variational function.

The following linear combination operator was introduced:

$$\begin{aligned} p_j &= \left[\frac{m\hbar\lambda}{2}\right]^{\frac{1}{2}} \left(b_j + b_j^{\dagger}\right), \\ r_j &= i\left[\frac{\hbar}{2m\lambda}\right]^{\frac{1}{2}} \left(b_j - b_j^{\dagger}\right), \end{aligned} \tag{9}$$

with λ being the variational parameter. The system ground-state wave function was written as

$$|\psi_0\rangle = |0\rangle_a |0\rangle_b, \tag{10}$$

where $|0\rangle_b$ and $|0\rangle_a$ are the vacuum state and unperturbed zero-phonon state of the b operator, respectively. The expected value of Equation (1) with respect to $|\psi_0\rangle$ was written as

$$F_0(\lambda, f_q) = \langle \psi_0 | U_2^{-1} U_1^{-1} H U_1 U_2 | \psi_0 \rangle \tag{11}$$

Performing the variation of $F_0(\lambda, f_q)$ with respect to λ gave

$$\lambda^2 - \frac{4\eta}{3\hbar}\sqrt{\frac{m}{\pi\hbar}}\lambda^{\frac{3}{2}} - \frac{V_0}{3mR^2} - \frac{\hbar e^2 B_0^2 \exp(-2\omega t)}{12m^2\lambda C^2} = 0 \tag{12}$$

where λ is the weak-coupling bound-polaron vibrational frequency in AGCPQWs. The GSBE and GSE of the bound polaron (GSEPB) were stated as

$$E_0 = \frac{3}{4}\hbar\lambda - \alpha\hbar\omega_{LO} - V_0 + \frac{\hbar V_0}{4m\lambda R^2} + \frac{\hbar e^2 B_0^2 \exp(-2\omega t)}{16m^2\lambda C^2} - 2\eta\sqrt{\frac{m\lambda}{\pi\hbar}} \tag{13}$$

$$E_b = 2\alpha\hbar\omega_{LO} + V_0 - \frac{\hbar V_0}{4m\lambda R^2} - \frac{\hbar e^2 B_0^2 \exp(-2\omega t)}{16m^2\lambda C^2} + 2\eta\sqrt{\frac{m\lambda}{\pi\hbar}} \tag{14}$$

3. Numerical Results and Discussion

To clearly determine the influences of the AGCP range, hydrogen-like impurities, and decay magnetic field on the GSBE and GSEPB in AGPQWs, numerical calculations for GaAs, InAs, and InSb semiconductor AGPQWs were performed. The parameters applied for calculations in experiments are shown in Table 1 [27].

Table 1. Parameters related to GaAs, InAs, and InSb crystals.

Crystal	α	ω_{LO}	m/m_e	m
InSb	0.022	5.72×10^{13} Hz	0.0138	1.26×10^{-32} kg
InAs	0.052	4.55×10^{13} Hz	0.0230	2.10×10^{-32} kg
GaAs	0.068	5.50×10^{13} Hz	0.0657	4.28×10^{-32} kg

To better discuss the aforementioned issue, different GaAs, InAs, and InSb crystal materials are presented in Figure 3, where the following physical quantities were selected: $V_0 = 3$ meV, $R = 1$ nm, $\omega = 0.5$ Hz, $T = 0.5$ s, and $B_0 = 4$ T. To compare the variations of the polaron ground-state energy in different crystals due to the Coulomb field of impurities, polaron ground-state energies of GaAs, InAs, and InSb crystal materials without impurities were calculated to be 56.233, 145.862, and 234.741 meV, respectively. Next, the energy variation ΔE_0 of the ground state of polarons in different materials was calculated as the Coulomb impurity potential strength changed. We found that by increasing the Coulomb potential, the variations of the ground-state energy ΔE_0 of polarons in different materials decreased. From the order of the coupling constants summarized in the table, it was seen that an increase in the coupling constant increased the polaron ground-state energy, indicating that stronger coupling between electrons and phonons results in a larger coupling constant in the crystal and in turn stronger binding of electrons and lower ground-state energy.

Similarly, in Figure 4, the GSBE change rule in Gaussian potential QWs of different GaAs, InAs, and InSb crystal materials varied with the Coulomb potential. On the one hand, this indicated that higher crystal material coupling constants result in stronger electron binding, higher polaron formation ground-state energy (i.e., the rule presented in Figure 3), and larger binding energy. On the other hand, by increasing the Coulomb potential, impurities greatly affect polarons. Therefore, it was equivalent to an extra electron-binding potential, which increased the polaron GSBE.

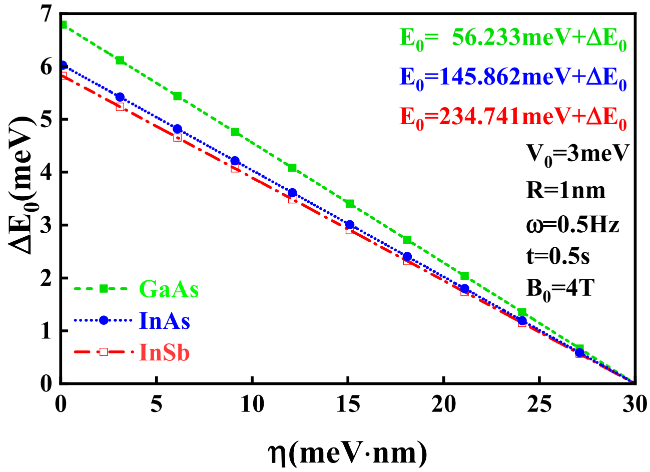

Figure 3. Change rules of the ground-state energy of GaAs, InAs, and InSb potential QWs with Coulombic impurities of different materials.

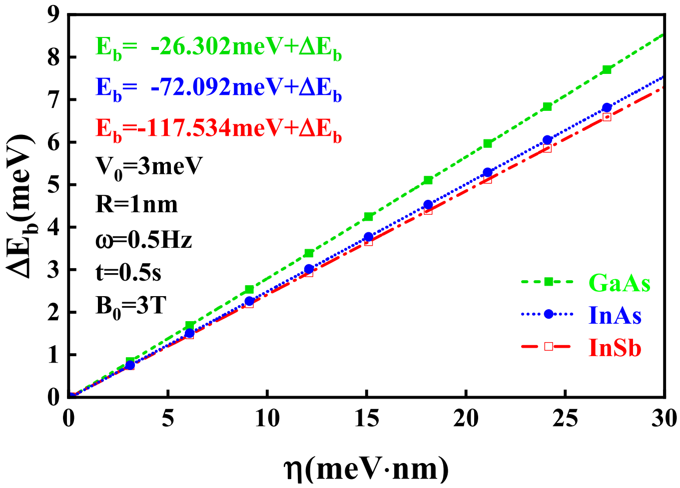

Figure 4. Change rules of the GSBE of GaAs, InAs, and InSb QWs with the Coulomb potential of different materials.

To clearly describe the effects of the potential and width of the self-parameter potential well in weakly coupled materials on the GSBE and the ground-state energy of polarons, we simulated the polaron-forming bound-magneto-polaron process under different magnetic fields, with $V_0 = 3$ meV, $\omega = 0.5$ Hz, $T = 0.5$ s, $B_0 = 4$ T, and impurity Coulomb field $\eta = 30$ meV $\cdot$ nm. As shown in the Figure 5, It was found that the bound-magneto-polaron ground-state energy increased by increasing the bound potential and decreased by increasing the well width. The larger the AGCP range is, the weaker the confinement ability of the electron, and the weaker the coupling between the electron and the phonon. As the well height of the AGCP increased, the confinement strength of the electrons increased in the growth direction of the QW, facilitating polaron formation. The change law of binding energy followed the opposite pattern. This was consistent with Figure 3.

As can be seen from Figure 6, this bound magneto-polaron was affected by the changing magnetic field, which changed the GSBE and ground-state energy of the polaron. To show this change, we also adopted a GaAs crystal material. Under QW parameters of $V_0 = 3$ meV, $R = 1$ nm, and Coulomb impurity field $\eta = 30$ meV·nm, we calculated the change rule of the bound magneto-polaron with related magnetic field parameters. The ground-state energy increased by increasing the initial magnetic field, and the negative value of the binding energy was consistent with that of the ground-state energy.

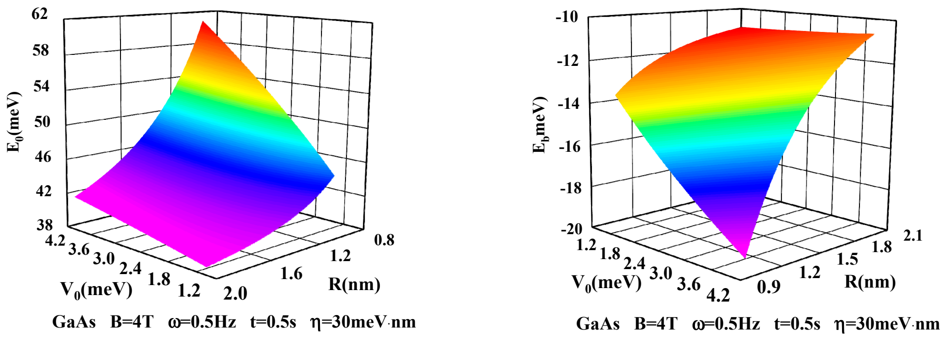

Figure 5. Variations of the ground-state energy of GaAs potential QWs of different materials with different magnetic fields and itself-parameters of QWs.

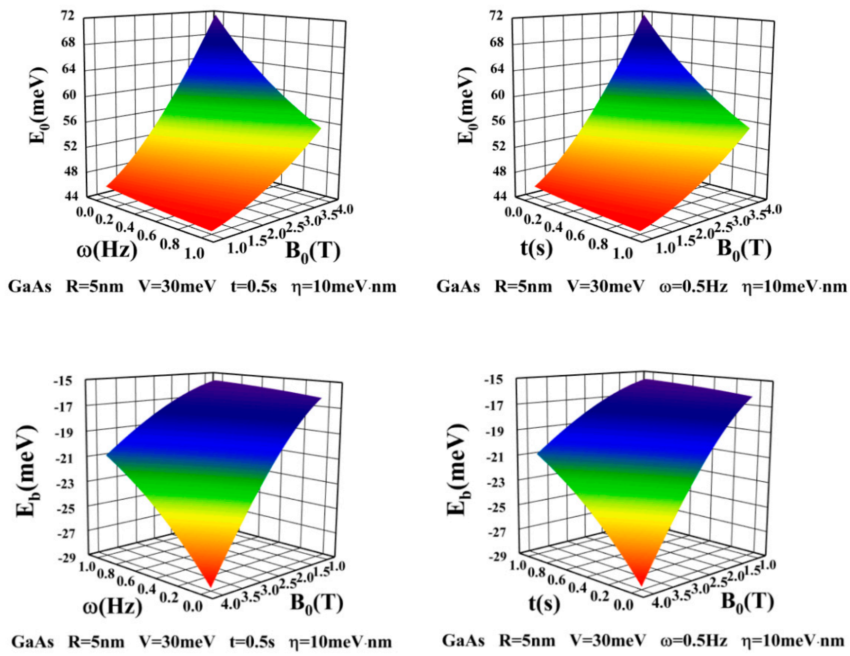

Figure 6. Change rules of the ground-state energy of GaAs Gaussian potential QWs with a changing magnetic field.

4. Conclusions

We studied the effects of the AGP range and hydrogen-like impurities on the GSBE, ground-state energy, and vibrational frequency of weak-coupling bound polarons in AGP III–V compound QWs based on unitary transformation and linear combination operator methods. The following conclusions can be drawn from numerical simulations: (1) The Coulomb impurity in the material enhances the polaron effect and then reduces the ground-state energy of the polaron. (2) The influence of Coulomb impurities on the polaron effect in different materials is obviously different, which may be caused by the different electronic–phonon coupling constant of materials. The larger the electronic–phonon coupling constant of materials, the more obvious the influence of Coulomb impurities. (3) The change in the confinement potentials has a significant influence on the polaron effect. With the increase in the confinement potentials, the electron–phonon interaction strength changes, leading to a change in the polaron energy. (4) The intensity of electron motion is enhanced by the influence of the magnetic field, resulting in an increase in the polaron energy. However, since the magnetic induction intensity of the decay field gradually decreases, the polaron energy in the decay field decreases and becomes more stable. The obtained results revealed that these factors have great effects on bound-polaron properties in AGP III–V compound

QWs, which can guide us to recognize, understand, and apply the polaron effect of AGP III–V compound QWs.

Author Contributions: Data curation, X.Z., W.Z. and X.-J.M.; Formal analysis, J.-L.X.; Funding acquisition, X.Z.; Investigation, W.Z., X.-J.M. and P.-F.L.; Methodology, Y.S.; Project administration, Y.S. and J.-L.X.; Writing—original draft, X.Z.; Writing—review & editing, Y.S. All authors have read and agreed to the published version of the manuscript.

Funding: The project is supported by the National Natural Science Foundation of China (12164032 and 11964026), the Natural Science Foundation of Inner Mongolia (2019MS01010 and 2020BS01009), the Doctor Research Start-up Fund of Inner Mongolia Minzu University (BS439), and Scientific Research Projects in Colleges and Universities in Inner Mongolia (NJZZ19145).

Institutional Review Board Statement: Not applicable.

Informed Consent Statement: Not applicable.

Data Availability Statement: Data is contained within the article.

Conflicts of Interest: The authors declare no conflict of interest.

References

1. Wang, L.; Li, W.; Yin, L.; Liu, Y.; Guo, H.; Lai, J.; Han, Y.; Li, G.; Li, M.; Zhang, J.; et al. Full-color fluorescent carbon quantum dots. *Sci. Adv.* **2020**, *6*, eabb6772. [CrossRef] [PubMed]
2. Dong, Y.; Wang, Y.-K.; Yuan, F.; Johnston, A.; Liu, Y.; Ma, D.; Choi, M.-J.; Chen, B.; Chekini, M.; Baek, S.-W.; et al. Bipolar-shell resurfacing for blue LEDs based on strongly confined perovskite quantum dots. *Nat. Nanotechnol.* **2020**, *15*, 668–674. [CrossRef] [PubMed]
3. Topnani, N.B.; Nagaraja, P.; Musevic, I.; Ramarao, P. Fluorescence intermittency and spatial localization of core-shell quantum rod clusters in an inverse nematic gel. *Phys. Rev. Mater.* **2020**, *4*, 126002. [CrossRef]
4. Cunha, S.M.; da Costa, D.R.; Felix, L.C.; Chaves, A.; Pereira, J.M., Jr. Electronic and transport properties of anisotropic semiconductor quantum wires. *Phys. Rev. B* **2020**, *102*, 045427. [CrossRef]
5. Tummuru, T.; Can, O.; Franz, M. Chiral p-wave superconductivity in a twisted array of proximitized quantum wires. *Phys. Rev. B* **2021**, *103*, L100501. [CrossRef]
6. Iyer, P.P.; DeCrescent, R.A.; Mohtashami, Y.; Lheureux, G.; Butakov, N.A.; Alhassan, A.; Weisbuch, C.; Nakamura, S.; DenBaars, S.P.; Schuller, J.A. Unidirectional luminescence from InGaN/GaN quantum-well metasurfaces. *Nat. Photonics* **2020**, *14*, 543–548. [CrossRef]
7. Olusola, O.I.; Shomotun, O.P.; Vincent, U.E.; McClintock, P.V.E. Quantum vibrational resonance in a dual-frequency-driven Tietz-Hua quantum well. *Phys. Rev. E* **2020**, *101*, 052216. [CrossRef]
8. Ridene, S. GaSbBi/GaSb quantum-well and wire laser diodes. *Chem. Phys. Lett.* **2018**, *702*, 44–48. [CrossRef]
9. Zhao, Q.; Aqiqi, S.; You, J.-F.; Kria, M.; Guo, K.-X.; Feddi, E.; Zhang, Z.-H.; Yuan, J.-H. Influence of position-dependent effective mass on the nonlinear optical properties in $Al_xGa_{1-x}As/GaAs$ single and double triangular quantum wells. *Phys. E Low-Dimens. Syst. Nanostruct.* **2020**, *115*, 113707. [CrossRef]
10. De Silva, N.; Warnakula, T.; Gunapala, S.D.; Stockman, M.I.; Premaratne, M. Effect of logarithmic perturbations in ohmic like spectral densities in dynamics of electronic excitation using variational polaron transformation approach. *J. Phys. Condens. Matter* **2021**, *33*, 145304. [CrossRef]
11. Asatryan, A.L.; Movsisyan, A.H.; Vartanian, A.L. External electric and magnetic field effects on the polaron in a wurtzite nitride nanowire embedded in a nonpolar matrix. *Eur. Phys. J. B* **2021**, *94*, 70. [CrossRef]
12. Bahar, M.K.; Rodríguez-Magdaleno, K.A.; Martínez-Orozco, J.C.; Mora-Ramos, M.E.; Ungan, F. Optical properties of a triple AlGaAs/GaAs quantum well purported for quantum cascade laser active region. *Mater. Today Commun.* **2021**, *26*, 101936. [CrossRef]
13. Yu, H.; Zhen, Z.; Shi, Y.-S.; Guo, K.-X.; Feddi, E.; Yuan, J.-H.; Zhang, Z.-H. The nonlinear optical absorption in AlxGa1−xAs/GaAs double-graded quantum wells: Magnetic field effect and the position-dependent effective mass effect. *Eur. Phys. J. Plus* **2021**, *136*, 555. [CrossRef]
14. Frankerl, C.; Nippert, F.; Gomez-Iglesias, A.; Hoffmann, M.P.; Brandl, C.; Lugauer, H.-J.; Zeisel, R.; Hoffmann, A.; Davies, M.J. Origin of carrier localization in AlGaN-based quantum well structures and implications for efficiency droop. *Appl. Phys. Lett.* **2020**, *117*, 102107. [CrossRef]
15. Gusev, G.M.; Olshanetsky, E.B.; Hernandez, F.G.G.; Raichev, O.E.; Mikhailov, N.N.; Dvoretsky, S.A. Two-dimensional topological insulator state in double HgTe quantum well. *Phys. Rev. B* **2020**, *101*, 241302. [CrossRef]
16. Donmez, O.; Aydın, M.; Ardalı, Ş.; Yıldırım, S.; Tıraş, E.; Nutku, F.; Çetinkaya, Ç.; Çokduygulular, E.; Puustinen, J.; Hilska, J.; et al. Electronic transport in n-type modulation-doped AlGaAs/GaAsBi quantum well structures: Influence of Bi and thermal annealing on electron effective mass and electron mobility. *Semicond. Sci. Technol.* **2020**, *35*, 025009. [CrossRef]

17. Sherly, I.J.; Nithiananthi, P. Tuning the dynamics of Bound Magnetic Polaron in asymmetric Cd1-x1Mnx1Te/Cd1-x2Mnx2Te Semimagnetic Concentric Double Quantum Rings: Through magnetic ion concentration and magnetic field. *Phys. B Condens. Matter* **2021**, *600*, 412615. [CrossRef]
18. Korshunova, A.N.; Lakhno, V.D. Charge Transfer by Polarons in a Homogeneous Poly G/Poly C-Chain Subjected to a Constant Electric Field in Terms of the Peyrard–Bishop–Holstein Model. *Tech. Phys.* **2020**, *65*, 1467–1474. [CrossRef]
19. Cai, C.-Y.; Qiu, W.; Sun, Y.; Zhao, C.-L.; Xiao, J.-L. Effects of an anisotropic parabolic potential and Coulomb's impurity potential on the energy characteristics of asymmetrical semi-exponential CsI quantum wells. *Commun. Theor. Phys.* **2021**, *73*, 015701. [CrossRef]
20. Selmi, M.; Smida, A.; El Kossi, S. Effect of Polaron formation in conduction and dielectric behavior in $La_{0.7}Sr_{0.25}K_{0.05}MnO_3$ oxide. *J. Mater. Sci. Mater. Electron.* **2021**, *32*, 6014–6027. [CrossRef]
21. Fobasso, M.F.C.; Fotue, A.J.; Kenfack, S.C.; Ekengue, C.M.; Ngoufack, C.D.G.; Akay, D.; Fai, L.C. Laser light and external magnetic field control of polaron in asymmetric quantum dot. *Superlattices Microstruct.* **2019**, *129*, 77–90. [CrossRef]
22. Phuc, H.V.; Tung, L.V.; Vinh, P.T.; Dinh, L. Nonlinear optical absorption via two-photon process in asymmetrical Gaussian potential quantum wells. *Superlatt. Microstruct.* **2015**, *77*, 267–275. [CrossRef]
23. Zhai, W. A study of electric-field-induced second-harmonic generation in asymmetrical Gaussian potential quantum wells. *Phys. B Condens. Matter* **2014**, *454*, 50–55. [CrossRef]
24. Wu, J.; Guo, K.; Liu, G. Polaron effects on nonlinear optical rectification in asymmetrical Gaussian potential quantum wells with applied electric fields. *Phys. B Condens. Matter* **2014**, *446*, 59–62. [CrossRef]
25. Lee, T.D.; Low, F.E.; Pines, D. The Motion of Slow Electrons in a Polar Crystal. *Phys. Rev.* **1953**, *90*, 297. [CrossRef]
26. Huybrechts, W.J. Internal excited state of the optical polaron. *J. Phys. C Solid State Phys.* **1977**, *10*, 3761. [CrossRef]
27. Gharaati, A.; Khordad, R. Effects of magnetic field and spin-orbit interaction on energy levels in 1D quantum wire: Analytical solution. *Opt. Quant. Electron.* **2012**, *44*, 425–436. [CrossRef]